Supporting Information

Rapid synthesis of magnetic microspheres and the development of new macro-micro hierarchically porous magnetic framework composites

John Luke Woodliffe[a], Jesús Molinar-Díaz[a], Md Towhidul Islam[a,b,c], Lee A. Stevens[a], Matthew D. Wadge[a], Graham A. Rance[d], Rebecca Ferrari[a], Ifty Ahmed[a], Andrea Laybourn[a]*

a) Faculty of Engineering, University of Nottingham, Nottingham, NG7 2RD, UK

b) School of Physical Sciences, University of Kent, Canterbury, UK

c) Department of Applied Chemistry and Chemical Engineering, Faculty of Engineering, Noakhali Science and Technology University, Noakhali, Bangladesh

d) Nanoscale and Microscale Research Centre (nmRC), Cripps South Building, University of Nottingham, Nottingham, NG7 2RD, UK

*Corresponding author. Email: andrea.laybourn@nottingham.ac.uk

Contents

1   Porous Magnetic Microspheres

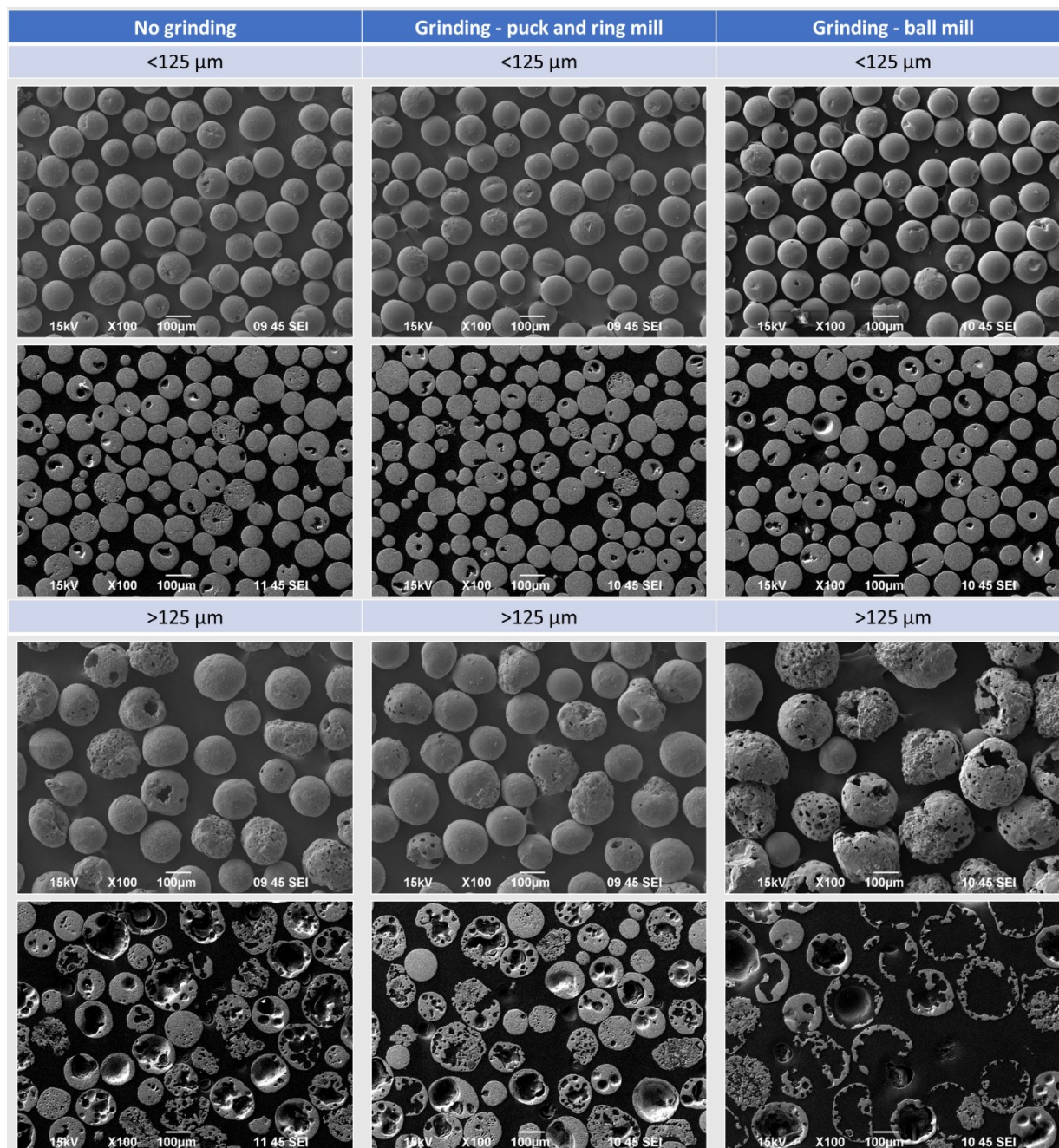## 1.1   SEM micrographs of varying mixing/grinding types

Figure S1. SEM micrographs of powders and cross sections of resultant porous magnetic microspheres produced without grinding and with grinding (of Fe_3O_4 with $CaCO_3$) using a puck and ring or ball mill. >125 µm and <125 µm fractions have been separated. Mixing in a

ball mill led to increased porosity compared with simple mixing without grinding (pestle and mortar) or grinding with a puck and ring mill.

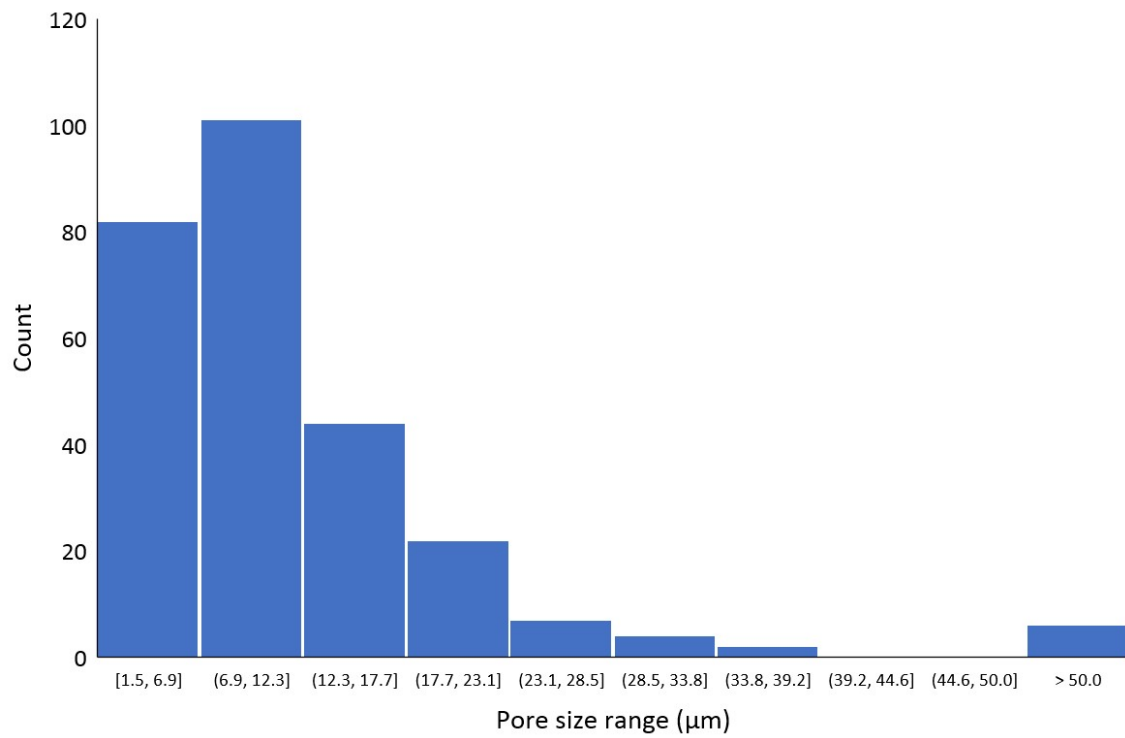## 1.2 Pore size distribution of high porosity microspheres

Figure S2. Histogram showing the size distribution of the pores in the porous microspheres by SEM image analysis.

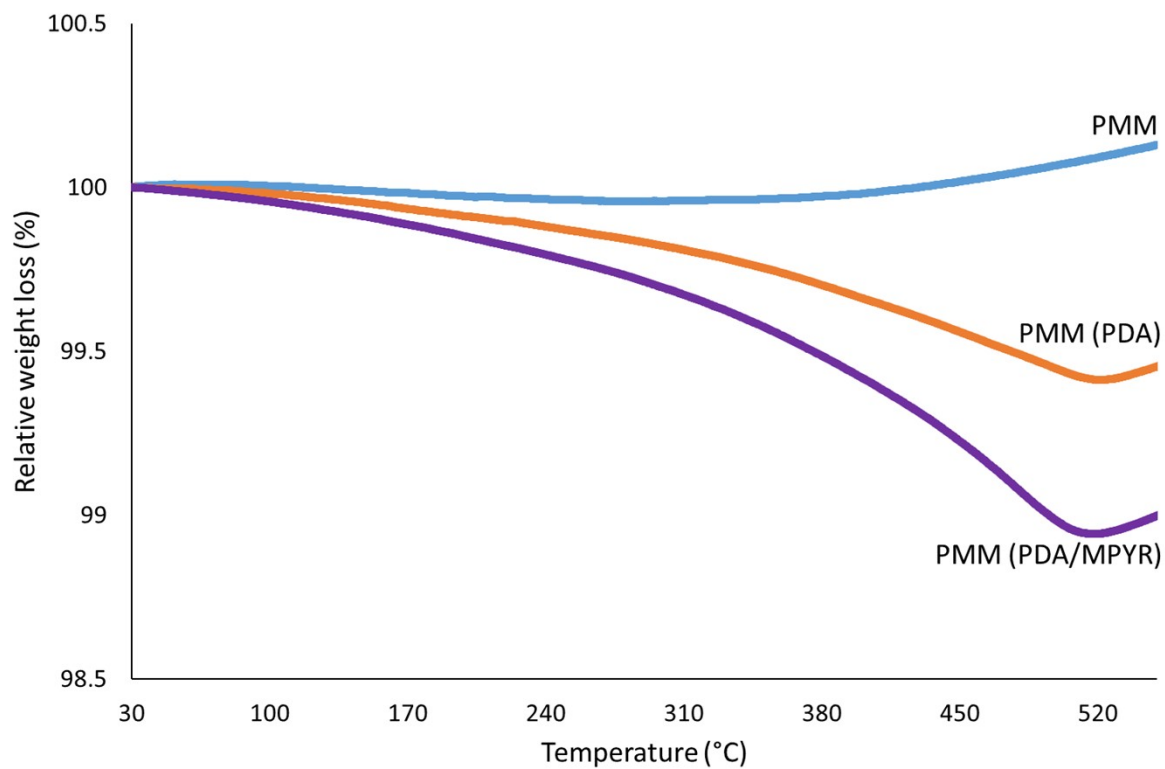# 2 Surface Functionalised Microspheres

2.1 TGA analysis

Figure S3. Thermal decompositions of unfunctionalised PMMs, and PMMs functionalised with PDA and PDA/MPYR.
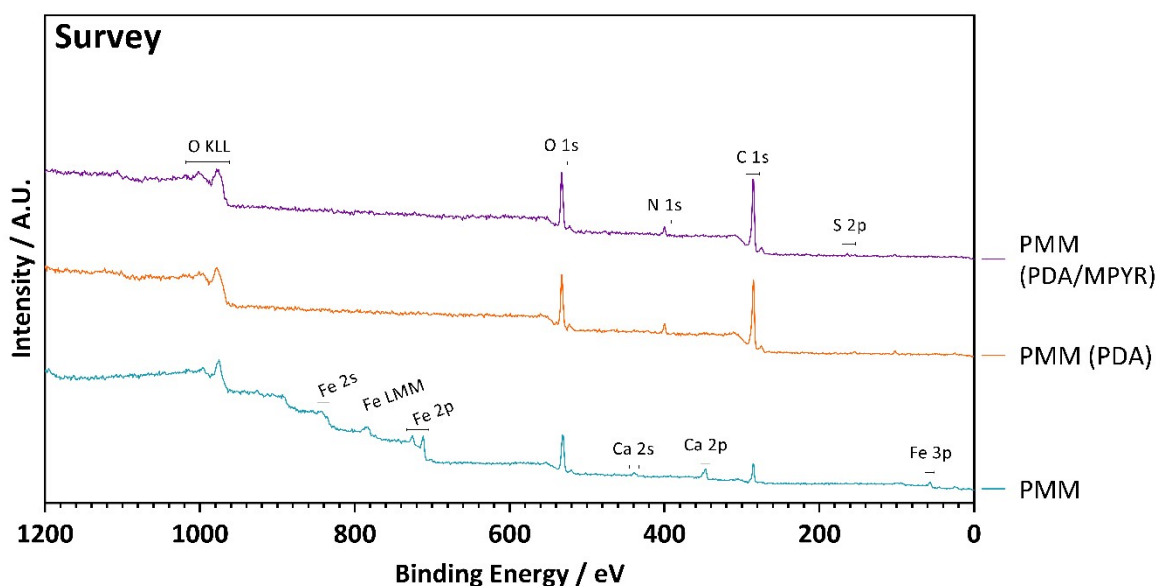
2.2 XPS analysis

Figure S4. Survey XPS spectra of unfunctionalised PMMs, and PMMs functionalised with PDA and PDA/MPYR.

A description of the full XPS deconvolutions, including relative atomic quantities, are presented below, and are summarised in Tables S1 and S2.

2.2.1 PMM

The O 1s high-resolution region was fitted to 2 peaks located at 530.2 (60.6%) and 532.2 (39.4%) eV corresponding to metallic oxides and water, respectively. C 1s spectrum was fitted to 3 peaks located at 284.8 (83.5%), 286.6 (7.3%) and 288.9 (9.3%) eV corresponding to adventitious carbon, C—O and C=O, respectively; the latter two being contamination arising from adventitious carbon interaction with oxygen and carbonates, respectively. Both Fe 2p and Ca 2p detailed doublet (j-j coupling) splits. Fe was found to be in its 3+ valence state due to the peak location of 710.8 eV ($\Delta_{ev} = 13.5$ eV) correlating with magnetite, with the presence of an additional peak between the two spin states, likely to be a Fe 2p satellite peak

(718.9 eV). Ca 2p demonstrated a single doublet split (3.5 eV shift), with peak location

(346.5 eV) corresponding to CaO.

2.2.2   PMM (PDA)

PDA layers are anticipated to be very thin (10s of nm[1,2]), and hence the presence of N 1s and

specific C peak fitted in XPS demonstrate a minimum bound on its thickness (5-10 nm). O 1s

again was fitted to 2 peaks; however, their locations at 531.2 (ca. 21%) and 532.6 (ca. 79%)

eV corresponded to C=O and C—O, respectively, compared to the native microspheres. The

binding energy at 532.6 eV is assigned to the oxygen from catechol and quinine form of

dopamine[3].   N 1s was fitted to a single peak located at 399.5 eV, corresponding to PDA

species[4,5]. C 1s, was fitted to 4 peaks; one more than the unfunctionalised microspheres. The

peaks presented were located at 284.4 (51.4%), 285.6 (33.6%), 287.2 (10.7%) and 288.9

(4.3%) eV, corresponding to C—C/CHx, C—N, C—O, and C=O, respectively[3,6].

2.2.3   PMM (PDA/MPYR)

Similar to the PDA microspheres, the O 1s spectral features were fairly consistent, except a

subtle shift of 0.2 eV for the O=C peak fit. No variations were seen in N 1s peak, however,

the C 1s did present subtle peak shifts and relative percentage differences, likely attributed to

the different chemical makeup of the surface due to MPYR deposition. 4 peak fittings, which

have shifted to 284.7, 285.7, 286.9, and 288.8 eV, with relative percentages of 68.6, 19.9, 6.8,

and 4.8 %, respectively, were observed. Most importantly for MPYR identification, the S 2p

region detailed a very low intensity doublet peak located at 163.3 eV, which due to the

variations in literature values, could either be correlated to unbonded thiol[7], which may be

surface dominant, rather than overall lack of S bonding to PDA moieties, or could be

attributed to S—C bonding[8].

Table S1. Atomic percentages of different elements in the microsphere samples obtained from fitting of XPS data.

Sample ID	Element (at.% ± S.E.M)					
	O	**N**	**C**	**S**	**Fe**	**Ca**
PMM	38.9 ± 1.0	-	47.9 ± 1.1	-	6.1 ± 0.6	7.0 ± 0.5
PMM (PDA)	20.4 ± 0.7	5.9 ± 0.7	73.7 ± 0.9	-	-	-
PMM (PDA/MPYR)	19.7 ± 0.6	4.8 ± 0.6	74.5 ± 0.8	1.0 ± 0.2	-	-

Table S2. Breakdown of XPS peaks in the microsphere samples, with their associated

binding energies, corresponding bonds and literature references.

Sample Code	Elements	Binding Energy / eV	Corresponding Bonds (Area / %)	Refs.
PMM	O 1s	530.2 532.2	M_x—O (60.6) O—H (39.4)	9
	C 1s	284.8 286.6 288.9	C—C/CH_x (83.5) C—O (7.3) C=O (9.3)	10
	Fe 2p	711.1 (2p 3/2) Shift Δ_{eV} = 13.5 eV	Fe(III)—O	9,11,12
	Ca 2p	346.5 (2p 3/2) Shift Δ_{eV} = 3.5 eV	Ca(II)—O	13
PMM (PDA)	O 1s	531.2 532.6	O=C (21.3) O—C (78.7)	4
	N 1s	399.7	N—H (100)	4,5
	C 1s	284.4 285.6 287.2 288.9	C—C/CH_x (51.4) C—N (33.6) C—O (10.7) C=O (4.3)	3,6
PMM (PDA/MPYR)	O 1s	531.0 532.6	C=O (21.5) C—O (78.5)	3,4

N 1s	399.5	N—H (100)	4,5
C 1s	284.7	C—C/CH$_x$ (68.6)	3,6
	285.7	C—N (19.9)	
	286.9	C—O (6.8)	
	288.8	C=O (4.8)	
S 2p	163.3 (2p 3/2) Shift Δ_{eV} = 1.2 eV	S—H or S—C	7,8,14

3   Magnetic Framework Composites

3.1   Synthesis of pristine MOF SIFSIX-3-Cu

Based on previously published method[15], a 5 mL pyrazine in methanol solution (0.300 g, 3.75 mmol) was layered onto a 5 mL CuSiF$_6$·H$_2$O in methanol solution (0.325 g, 1.45 mmol) and left at room temperature for 24 hours in a glass vial. The product was collected by centrifuge and washed with methanol (40 mL x 3) before drying in an oven at 50 °C for 2 hours.
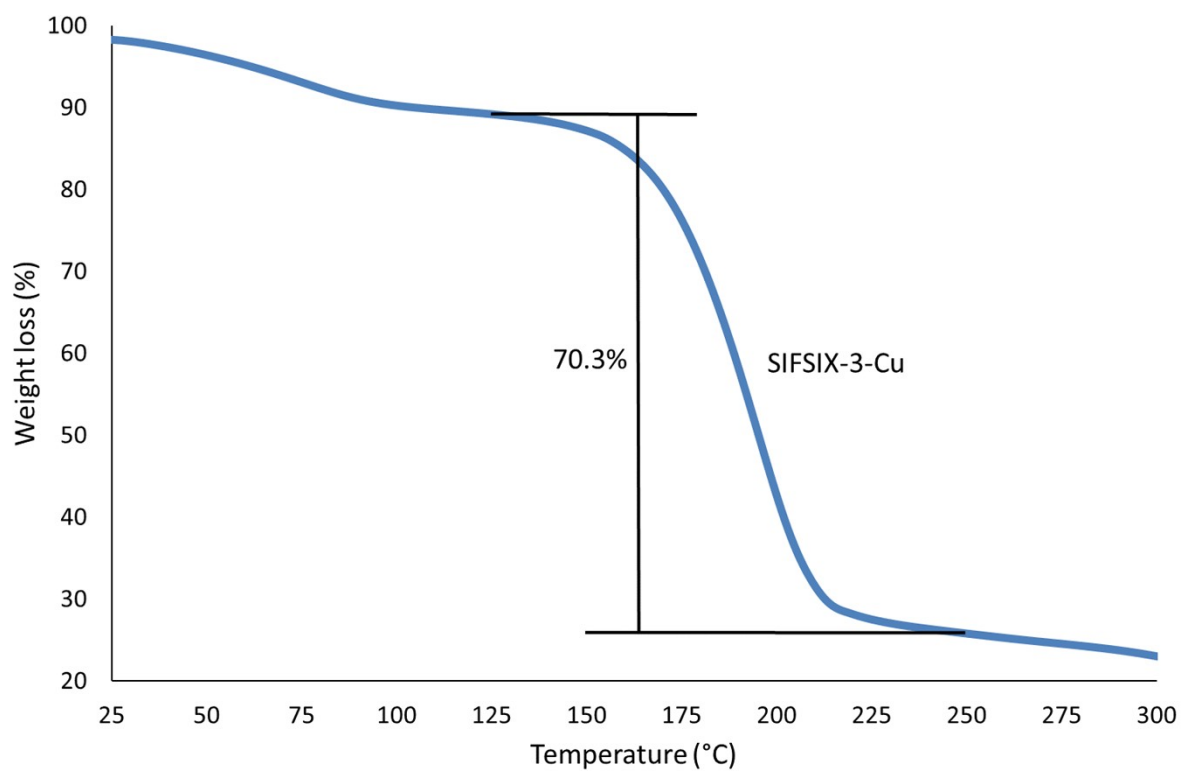
3.2 TGA of pristine MOF SIFSIX-3-Cu

Figure S5. Thermal decomposition of MOF SIFSIX-3-Cu under N_2 gas at a 10 °C/min ramp rate. Main decomposition between 125 and 250 °C characterised as a 70.3% weight loss when normalised for moisture content.
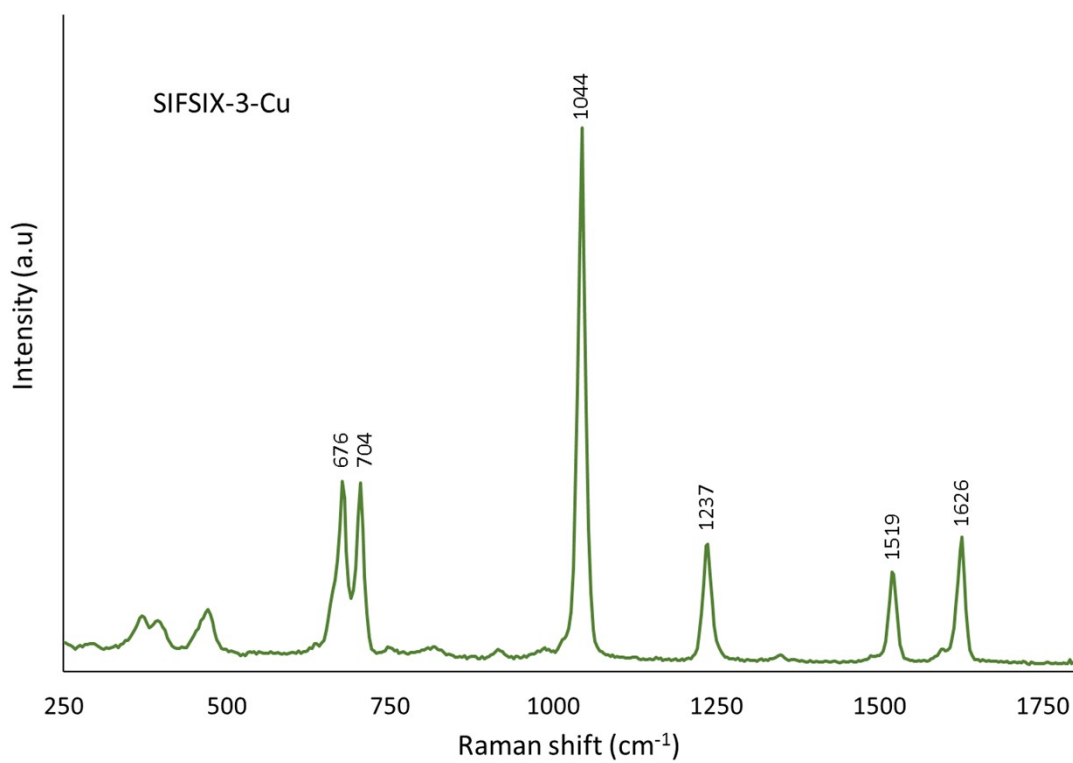
3.3 Raman analysis of pristine MOF SIFSIX-3-Cu

Figure S6. Raman spectrum of pristine MOF SIFSIX-3-Cu.
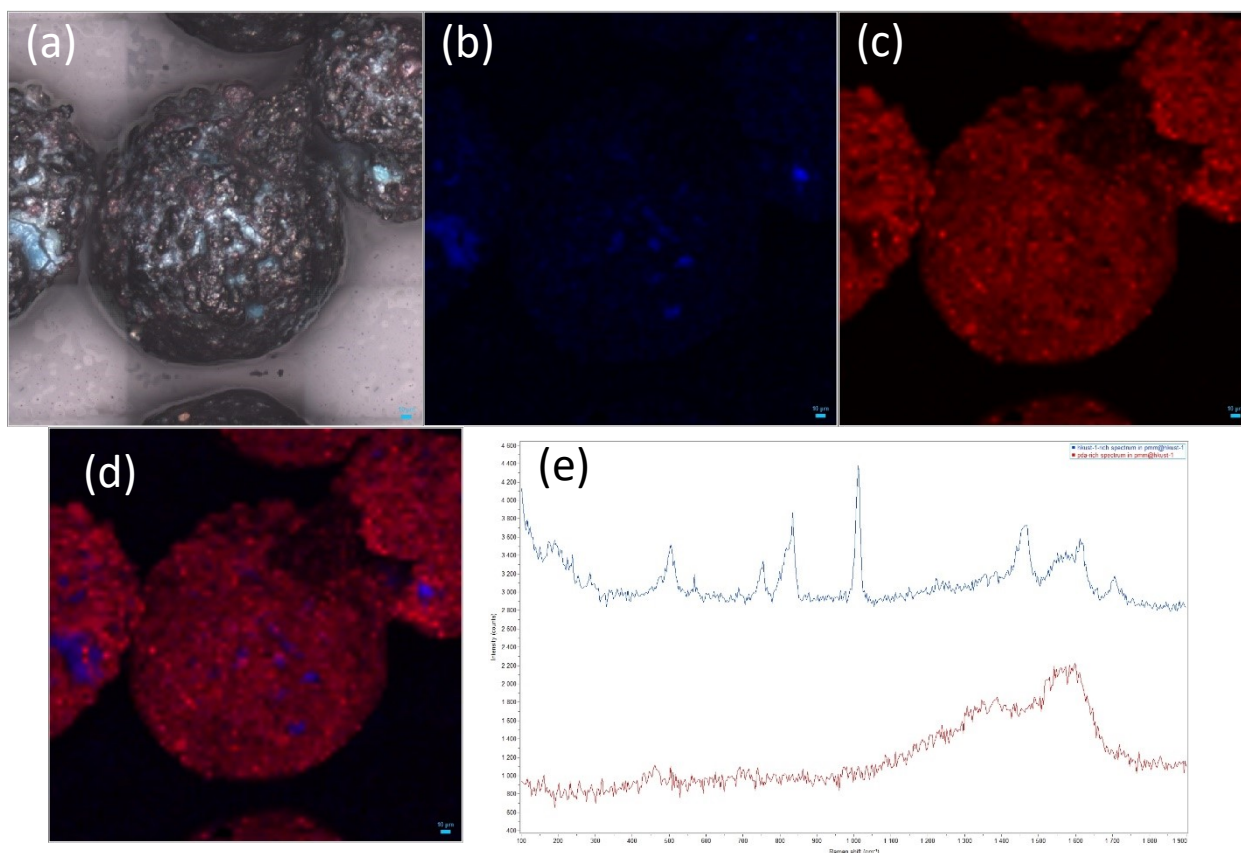
3.4   Raman mapping of MFCs

Figure S7. Confocal Raman microscopy analysis of HKUST-1@PMM (PDA). Blue scale

bar in bottom right is 10 μm. (a) Optical micrograph and (b-d) Raman maps of a typical

HKUST-1-coated PMM. The blue map (b) shows the intensity of the band within the range

960-1060 cm^{-1} (* centred at 1011 cm^{-1}) diagnostic of HKUST-1 (assigned as an in-plane

bending mode of the aromatic ring of the benzene-1,3,5-tricarboxylate linker, $\delta(\text{C-C-C})_R$)[16]. It

is important to note that areas of blue colouration in (b) closely match areas of sky blue

colouration in the optical image (a). The red map (c) shows the intensity of the bands within

the range 1100-1800 cm^{-1} (**) diagnostic of PDA[17]. In (d) the blue and red maps are overlaid,

with the intensities normalised for visual impact. Scale bars in (a-d) are 10 microns. (e)

Representative point spectra from HKUST-1-rich (top, blue trace) and PDA-rich (bottom, red

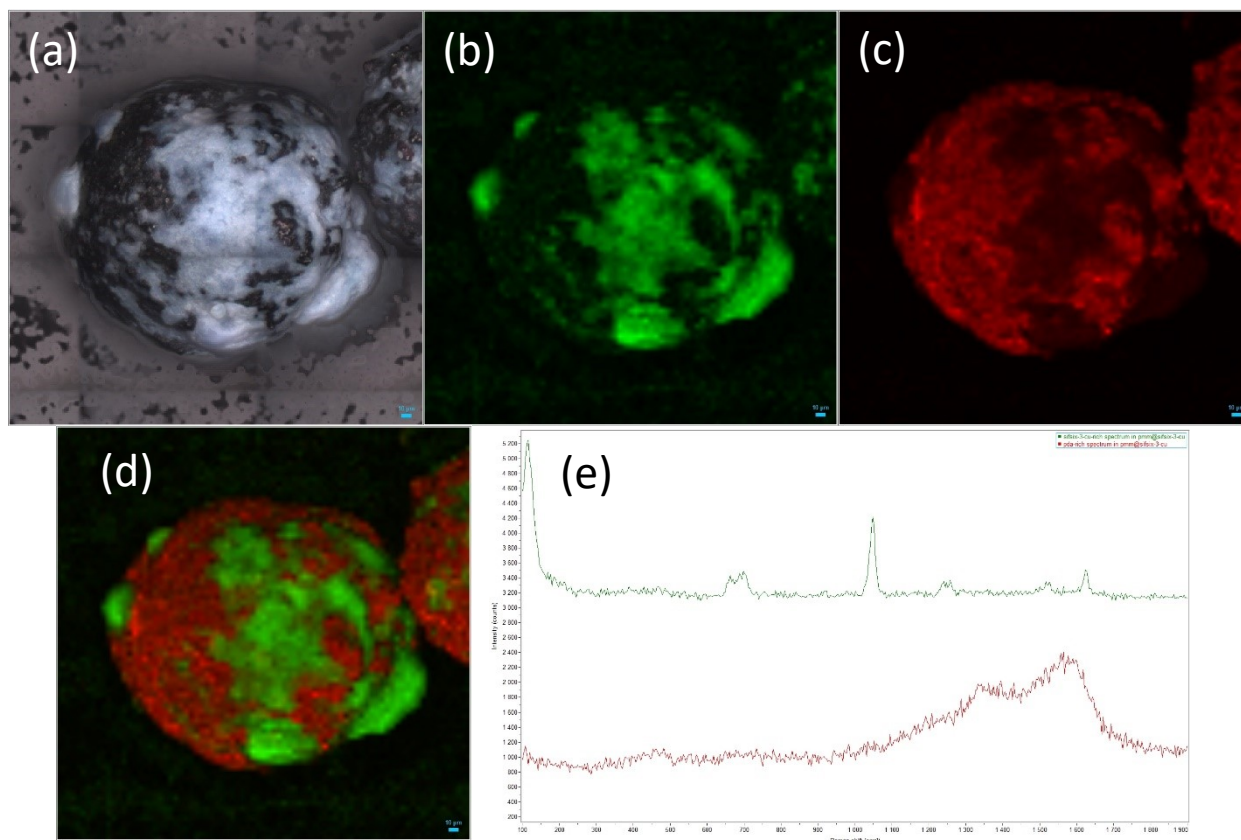trace) areas of the assessed microsphere. Spectra have been offset on the y-axis for ease of comparison.

Figure S8. Confocal Raman microscopy analysis of SIFSIX-3-Cu@PMM (PDA/MPYR). Blue scale bar in bottom right is 10 μm. (a) Optical micrograph and (b-d) Raman maps of a typical SIFSIX-3-Cu-coated PMM. The green map (b) shows the intensity of the band within the range 990-1100 cm^{-1} (*, centred at 1046 cm^{-1}) diagnostic of SIFSIX-3-Cu (tentatively assigned as a ring bending mode of the pyrazine linker, based on prior reports of structural analogues)[18]. It is important to note that areas of green colouration in (b) closely match areas of white colouration in the optical image (a). The red map (c) shows the intensity of the bands within the range 1100-1800 cm^{-1} (**) diagnostic of PDA[17]. In (d) the green and red maps are overlaid, with the intensities normalised for visual impact. Scale bars in (a-d) are 10 microns.

(e) Representative point spectra from SIFSIX-3-Cu-rich (top, green trace) and PDA-rich (bottom, red trace) areas of the assessed microsphere. Spectra have been offset on the y-axis for ease of comparison.

4 References

1   H. Hantsche, *Scanning*, 1989, **11**, 257–280.

2   H. Lee, S. M. Dellatore, W. M. Miller and P. B. Messersmith, *Science (80-.).*, 2007, **318**, 426–430.

3   Z.-Y. Xi, Y.-Y. Xu, L.-P. Zhu, Y. Wang and B.-K. Zhu, *J. Memb. Sci.*, 2009, **327**, 244–253.

4   A. J. Parsons, R. M. Felfel, M. D. Wadge and D. M. Grant, *Int. J. Appl. Glas. Sci.*, 2020, **11**, 35–45.

5   R. M. Felfel, A. J. Parsons, M. Chen, B. W. Stuart, M. D. Wadge and D. M. Grant, *Compos. Part A Appl. Sci. Manuf.*, 2021, **146**, 106415.

6   H. Lee, W.-J. Lee, Y.-K. Park, S. J. Ki, B.-J. Kim and S.-C. Jung, *Nanomater.* , 2018, 8.

7   D. G. Castner, K. Hinds and D. W. Grainger, *Langmuir*, 1996, **12**, 5083–5086.

8   H. Marsh, P. M. A. Sherwood and D. Augustyn, *Fuel*, 1976, **55**, 97–98.

9   A. P. Grosvenor, B. A. Kobe, M. Biesinger and N. Mcintyre, *Surf. Interface Anal.*, 2004, **36**, 1564–1574.

10   J. Stoch and J. Gablankowska-Kukucz, *Surf. Interface Anal.*, 1991, **17**, 165–167.

11   A. Rajan, M. Sharma and N. K. Sahu, *Sci. Rep.*, 2020, **10**, 15045.

12   M. Sinhababu, A. Roy, N. Kumar, M. Dutta, S. Sundaram, S. Karazhanov and G. Udayabhanu, *Nanomater.* , 2021, 11.

13 M. I. Sosulnikov and Y. A. Teterin, *J. Electron Spectros. Relat. Phenomena*, 1992, **59**, 111–126.

14 S. Herrera, F. Tasca, F. J. Williams, E. J. Calvo, P. Carro and R. C. Salvarezza, *Langmuir*, 2017, **33**, 9565–9572.

15 O. Shekhah, Y. Belmabkhout, Z. Chen, V. Guillerm, A. Cairns, K. Adil and M. Eddaoudi, *Nat. Commun.*, 2014, **5**, 4228.

16 F. S. Gentile, M. Pannico, M. Causà, G. Mensitieri, G. Di Palma, G. Scherillo and P. Musto, *J. Mater. Chem. A*, 2020, **8**, 10796–10812.

17 H. Li, Y. V Aulin, L. Frazer, E. Borguet, R. Kakodkar, J. Feser, Y. Chen, K. An, D. A. Dikin and F. Ren, *ACS Appl. Mater. Interfaces*, 2017, **9**, 6655–6660.

18 P. Kanoo, S. K. Reddy, G. Kumari, R. Haldar, C. Narayana, S. Balasubramanian and T. K. Maji, *Chem. Commun.*, 2012, **48**, 8487–8489.